Interaction of YAP with the Myb-MuvB (MMB) complex defines a transcriptional program to promote the proliferation of cardiomyocytes

Marco Gründl[1], Susanne Walz[2], Laura Hauf[1], Melissa Schwab[1], Kerstin Marcela Werner[1], Susanne Spahr[1], Carsten P. Ade[1] and Stefan Gaubatz[1*]

[1]Theodor Boveri Institute and Comprehensive Cancer Center Mainfranken, Biocenter University of Wuerzburg, Wuerzburg, 97074, Germany

[2]Comprehensive Cancer Center Mainfranken, Core Unit Bioinformatics, Biocenter, University of Wuerzburg, Wuerzburg, 97074, Germany

[*]Correspondence to:

Stefan Gaubatz

Phone (+49) 931-31-84138

e-mail:stefan.gaubatz@biozentrum.uni-wuerzburg.de

SUMMARY

YAP, a major downstream effector of the Hippo signaling pathway, is an important regulator of cell proliferation. The ability of YAP to regulate G2/M gene expression is dependent on the Myb-MuvB (MMB) complex, consisting of the evolutionary MuvB core complex and the facultative B-MYB subunit, a transcription factor. Here we show that YAP directly binds to B-MYB. Disruption of the YAP/B-MYB interaction by overexpression of the YAP binding domain of B-MYB results in errors in cell division. We also show that YAP and MMB interact *in vivo* in the developing heart. Genome studies revealed that YAP and MMB regulate an overlapping set of cell cycle genes in cardiomyocytes. Cardiac specific deletion of the LIN9 subunit of MMB prevents the upregulation of cell cycle genes and the increased proliferation of cardiomyocytes lacking the Hippo-signaling component SAV1. Similarly, we find that proliferation of postnatal cardiomyocytes induced by constitutive active YAP depends on MMB. Our findings provide new insights in the YAP induced proliferation of cardiomyocytes through the functional interaction with MMB.

INTRODUCTION

The correct regulation of the cell cycle is essential for normal development and, when disturbed, can lead to a number of diseases. Changes in transcriptional activity ensure that proteins required for different cell-cycle phases or developmental states are produced at the correct time. The evolutionary conserved MuvB multiprotein complex functions as one of the transcriptional regulators of cell cycle genes (Sadasivam & DeCaprio, 2013; Fischer & Müller, 2017). Dependent on its interactions with different binding partners, MuvB can either repress or activate transcription. Specifically, when MuvB, consisting of the five proteins LIN9, LIN52, LIN54, LIN37 and RBBP4, interacts with the p130 retinoblastoma protein paralog, and with E2F4 and DP1, it forms the DREAM complex, which represses E2F-dependent gene expression in quiescent cells and in early G1 (Litovchick *et al*, 2007; Schmit *et al*, 2007). Upon cell cycle entry, p130, E2F4 and DP1 dissociate from the complex and the MuvB core

associates with the transcription factor B-MYB (Sadasivam *et al*, 2012; Pilkinton *et al*, 2007; Schmit *et al*, 2007; Osterloh *et al*, 2007). This Myb-MuvB (MMB) complex activates a set of genes required for mitosis and cytokinesis.

We recently observed that MMB and the transcriptional coactivator YAP co-regulate an overlapping set of late cell cycle genes (Pattschull *et al*, 2019). The activity of YAP and related TAZ is controlled by the highly conserved Hippo pathway, a kinase cascade, that regulates proliferation and organ size during development (Hong & Guan, 2012). When the Hippo pathway is active, the upstream MST1/2 kinases together with Salvador (SAV1) phosphorylate and activate the terminal LATS1/2 kinase (Meng *et al*, 2016). LATS1/2 in turn phosphorylate YAP and TAZ, which results either in cytoplasmic retention by 14-3-3 proteins or SCF-mediated proteasomal degradation of YAP/TAZ (Meng *et al*, 2016). In contrast, when Hippo is inactive, YAP/TAZ enter the nucleus and act as transcriptional coactivators predominantly by binding to DNA through TEAD transcription factors. Recent genome wide studies revealed that YAP/TEAD preferentially binds to distant enhancers (Zanconato *et al*, 2015; Galli *et al*, 2015; Stein *et al*, 2015). The binding of YAP to enhancers of G2/M genes promotes the chromatin-association of B-MYB to MMB-bound promoters through chromatin-looping, providing an explanation for the co-activation of late cell cycle genes by YAP and MMB (Pattschull *et al*, 2019).

The Hippo pathway and its downstream effectors YAP and TAZ are involved in cardiac development and has been implicated in heart regeneration after tissue damage (Liu & Martin, 2019; Wang *et al*, 2018). For example, cardiac-specific deletion of the Hippo kinases LATS1/2 or the scaffold protein SAV1 results in heart enlargement and increased proliferation of embryonal and postnatal cardiomyocytes due to increased YAP activity (Heallen *et al*, 2011; Heallen *et al*, 2013). Furthermore, expression of active YAP promotes proliferation of postnatal cardiomyocytes and induces a fetal-like cell state in adult cardiomyocytes (Gise *et al*, 2012; Monroe *et al*, 2019). Conversely, deletion of YAP in the embryonic heart reduces cardiomyocyte proliferation and results in myocardial hypoplasia and embryonic lethality (Xin *et al*, 2011). Recent studies also demonstrate that Hippo-deficient mice or mice expressing

active YAP show a better outcome after myocardial infarction (Heallen *et al*, 2013; Morikawa *et al*, 2015; Leach *et al*, 2017; Xin *et al*, 2013; Lin *et al*, 2014). Together, these studies identify YAP as an important regulator of cardiomyocyte proliferation and cardiac regeneration.

Whether the crosstalk between YAP and MMB contributes to cardiomyocyte proliferation during cardiac development has not yet been investigated.

In the current study, we demonstrate the WW-domains of YAP directly interact with a newly identified YAP-binding domain in the N-terminal part of B-MYB. Based on the binding studies we designed a fragment of B-MYB, MY-COMP, that can interfere with the YAP-B-MYB association. Expression of MY-COMP results in errors in cell division highlighting the importance of the YAP-MMB interaction for normal cell cycle progression. We further show that YAP and MMB interact in developing cardiomyocytes. Genetic studies indicate that this interaction is essential for increased mitosis of Hippo-deficient cardiomyocytes. Additionally, we demonstrate that YAP driven proliferation of postmitotic cardiomyocytes is dependent of MMB. Together, our data suggests that the YAP-MMB interaction is essential for cell cycle progression of cardiomyocytes, underscoring the functional relevance of the crosstalk between these two pathways for proper heart development.

RESULTS

B-MYB interacts with the tandem WW domains of YAP

The Hippo coactivator YAP interacts with the B-MYB subunit of the MMB complex in mammalian cells to regulate the expression of cell cycle genes (Pattschull *et al*, 2019). To gain further insights into the interplay between YAP and MMB and to develop tools to interfere with the interaction, we mapped the domain of YAP that is required for its ability to bind to B-MYB. To do so, we performed co-immunoprecipitation experiments with HA-B-MYB and a set of truncated flag-tagged YAP constructs.

In these assays, B-MYB interacted with YAP only when the tandem WW domains were present. B-MYB did not interact with the C-terminal transactivation domain or the PDZ-binding motif (Figure 1A,B,C). Internal deletion of the tandem WW domains abolished the binding, confirming that these domains are required for the YAP-B-MYB interaction (Figure 1D). To verify that the YAP WW domains mediate the interaction with B-MYB, we performed pulldown experiments with recombinant GST fused to the N-terminal part of YAP containing the TEAD-binding and WW domains (GST-TEAD-WW1/2) or just the two WW domains (GST-WW1/2) (Figure 1E). Recombinant GST-proteins were incubated with extracts of HeLa cells expressing HA-tagged B-MYB and bound B-MYB was detected by immunoblotting with an anti-HA antibody. In these experiments, HA-B-MYB specifically bound to GST-TEAD-WW1/2 and GST-WW1/2 and but not to GST alone (Figure 1F). YAP binds to DNA mainly by binding to TEAD transcription factors. We therefore used HA-tagged TEAD4 as a positive control. HA-TEAD4 only bound to GST-TEAD-WW1/2 containing the TEAD-binding domain, but not to GST alone or to GST-WW1/2. HA-tagged EB1, which was used as a negative control, did not bind to any of the GST constructs. Using GST-fusion proteins containing either one of the two WW domains (GST-WW1 and GST-WW2), we found that B-MYB can independently bind to both WW domains (Figure 1G). However, B-MYB more strongly interacted with the first WW domain and strongest binding of B-MYB was observed when both WW domains were present (Figure 1G).

B-MYB binds to the WW domains of YAP through a PPXY motif

We have previously shown that the N-terminal part of B-MYB comprised of the amino acids 1-410, but not the C-terminus from 411-700, interacts with YAP (Pattschull *et al*, 2019). Since the MMB-interaction domain (MBD) is located in the C-terminal region of B-MYB, this result suggested that the binding of YAP to B-MYB is not mediated by binding of YAP to the MuvB core (Guiley *et al*, 2015). We now wanted to map the region of B-MYB that binds to YAP more precisely and we asked whether B-MYB directly binds to YAP.

Pulldown experiments with GST-WW1 and with a set of HA-tagged B-MYB deletion mutants revealed that the minimal binding site for YAP is located between amino acids 80 and 241 of B-MYB (Figure 2A,B). For example, B-MYB(2-241) robustly bound to YAP whereas B-MYB(2-79) and B-MYB(242-410) failed to bind to YAP (Figure 2B). The interaction between B-MYB and YAP could be indirect since exogenously expressed HA-B-MYB likely associates with additional cellular proteins. To test whether the interaction between B-MYB and YAP is direct, we incubated purified, recombinant his-tagged B-MYB(2-241) with GST-WW1, GST-WW2 or with GST-WW1/2. Purified his-B-MYB(2-241) specifically interacted with GST-WW1/2, but not with GST, indicating that the binding between B-MYB and YAP is direct (Figure 2C). Recombinant his-B-MYB bound only weakly to the individual WW domains, consistent with the weaker binding of HA-tagged B-MYB to the single WW domains compared to the tandem WW domains (Figure 2C, see Figure 1G). This indicates that both WW domains are necessary for an efficient interaction with B-MYB.

The WW domain is a protein-interaction domain characterized by two tryptophan-residues separated by 20 to 22 amino acids. Ligands for the WW domain are proline-rich regions such as the PPXY motif (Macias *et al*, 2015; Chen & Sudol, 1995). B-MYB harbors a PPXY sequence (PPVY) between the N-terminal DNA-binding domain and the central transactivation domain (Figure 2A). Importantly, this PPXY motif is located in the region of B-MYB that was found to interact with YAP, leading to the hypothesis that it is involved in binding to YAP. We directly tested this idea by performing pulldown experiments with a deletion mutant of recombinant B-MYB lacking the PPXY sequence (ΔPPXY). Compared to his-tagged B-MYB(2-241), binding of his-B-MYB(2-241,ΔPPXY) to the WW domains of YAP was strongly reduced (Figure 2D). To investigate whether the PPXY motif is also required for the interaction with YAP in the context of the full-length B-MYB protein in cells, we next performed co-immunoprecipitation experiments of flag-tagged YAP with HA-B-MYB and with HA-B-MYB(ΔPPXY). Binding of B-MYB to YAP was again strongly reduced when the PPXY sequence was deleted (Figure 2E,F). Taken together, these results indicate that the YAP

interacting region of B-MYB is located between amino acid 80 and 241 of B-MYB and involves a PPXY motif.

Overexpression of the YAP binding domain disrupts the B-MYB-YAP interaction and results in errors in cell division

Since B-MYB and YAP directly interact, we next asked whether overexpression of the YAP binding domain of B-MYB can interfere with the interaction of B-MYB with YAP due to steric hindrance (Figure 3A). To address this possibility we created B-MYB(2-241) fused to a HA tag and a nuclear localization signal (HA-NLS-B-MYB-2-241), and named it MY-COMP for MYB-YAP competition. First, we expressed MY-COMP in HeLa cells and performed co-immunoprecipitation experiments. In cells that express MY-COMP, the amount of full length HA-B-MYB co-precipitating with flag-YAP was strongly reduced when compared to control transfected cells (Figure 3B,C). Expression of MY-COMP also interfered with the endogenous YAP and B-MYB interaction as determined by proximity ligation assays (PLA) (Figure 3D,E). Strikingly, expression of MY-COMP resulted in a pronounced increase in bi- and multinucleated cells and in cells with micronuclei (Figure 3G,H). Importantly, a shortened version of MY-COMP (HA-NLS-B-MYB(2-79)), which does not bind to YAP showed no such effect. The effect of MY-COMP is not due to interference with the DNA-binding of B-MYB, because expression of MY-COMP with a mutation in the DNA-binding domain that has been shown to prevent the interaction with DNA (Werwein *et al*, 2012), showed the same phenotype (Figure 3H). Importantly, deletion of the PPXY motif in MY-COMP abolished the effect on bi- and multinucleation and decreased micronuclei formation, indicating that the ability to induce cell division errors correlates with the ability to disrupt the YAP-B-MYB interaction. B-MYB constructs were expressed at comparable levels and we did not find any changes in B-MYB and YAP expression levels and in YAP-phosphorylation at S127 in these cells (Figure 3F). Phosphorylation of S127 was used as a proxy for YAP activity as it is a key residue for phosphorylation by the Hippo kinases LATS1/2. Taken together, these experiments provide evidence for the importance of the B-MYB-YAP interaction for normal cell cycle progression.

YAP interacts with MMB in cardiomyocytes

We next asked whether the interaction between B-MYB and YAP is of relevance *in vivo*. YAP is known to promote proliferation of embryonic cardiomyocytes during development whereas inhibition of YAP by the Hippo cascade suppresses cardiomyocyte proliferation (Heallen *et al*, 2011; Xin *et al*, 2011; Gise *et al*, 2012). Activated YAP or loss of Hippo signaling can also extend the neonatal proliferation of cardiomyocytes to postnatal stages, where proliferation is normally very low (Gise *et al*, 2012; Heallen *et al*, 2011; Monroe *et al*, 2019). Whether MuvB impacts on the ability of YAP to regulate cardiomyocyte gene expression and to promote cardiomyocyte proliferation is unclear. We first investigated whether YAP and B-MYB interact in the heart. PLA showed that YAP indeed interacted with B-MYB in developing cardiomyocytes (Figure 4A,B). The interaction was specific, as demonstrated by the loss of the PLA signal upon siRNA-mediated depletion of B-MYB (Figure 4A,B). YAP also interacted with LIN9, a core subunit of the MuvB complex that is required for binding of B-MYB to MuvB (Guiley *et al*, 2018), providing further evidence for an interaction between YAP and MMB in cardiomyocytes.

Hippo and MMB regulate an overlapping set of genes in embryonic cardiomyocytes

To explore the connection between the Hippo-YAP pathway and MMB *in vivo* in the heart, we deleted the Hippo pathway member Salvador (*Sav1*), a scaffold protein that is required for Hippo kinase activity, and the MMB subunit *Lin9* in cardiac precursor cells. Cardiac specific deletion of *Lin9* and *Sav1* was achieved by using mouse strains with conditional (floxed) alleles of *Sav1* and *Lin9* in combination with Nkx2.5-Cre (Cai *et al*, 2010). Phosphorylation of YAP on S127 was reduced, indicating that YAP is hyperactivated in *Sav1* deficient hearts (Supplementary Figure S1A). First, we explored the impact of *Lin9* mutation on the transcriptional program of Hippo-deficient cardiomyocytes by performing RNA-seq using RNA isolated from embryonic heart ventricles of mice carrying cardiac specific deletions of *Sav1* alone, *Lin9* alone or *Sav1* and *Lin9* together.

In *Sav1* knockout hearts, E2F target genes and other gene sets related to cell cycle regulation were enriched after inactivation of Hippo-signaling (Figure 5A, Supplementary Figure S1B). Strikingly, the activation of these gene sets was suppressed by the simultaneous deletion of *Lin9* together with *Sav1*, indicating that the elevated expression of these genes in *Sav1* mutant hearts requires the function of MMB (Figure 5A,B, Supplementary Figure S1B). By qPCR we independently validated that a set of cell cycle target genes were activated in *Sav1* mutated hearts, downregulated in *Lin9* mutated hearts and remained downregulated in hearts isolated from double mutant embryos (Figure 5C).

To find out whether cell cycle genes upregulated in *Sav1* hearts are direct targets of MMB, we performed chromatin immunoprecipitation experiments followed by high-throughput sequencing (ChIP-seq). We identified 3357 bindings sites for LIN9 in the fetal heart and 2672 binding sites in the postnatal heart. While the reduced expression of LIN9 in postnatal hearts likely contributes to the lower number of LIN9 sites in postnatal hearts (see below), the overall binding pattern of LIN9 was similar at the two developmental time points and the shared binding sites reflect high confident LIN9-binding sites (Figure 5D, Supplementary Figure S1C). By comparison with previously reported ChIP-seq data of histone modifications characteristic for active promoters and enhancers, most LIN9 binding sites are located in active promoters while less than 5% of LIN9 sites are found in enhancers or super-enhancers (Figure 5E, Supplementary Figure S1C).

To identify the direct targets of LIN9 in the heart, we plotted changes in gene expression upon deletion of *Lin9* against the density of promoter-bound LIN9. This revealed a correlation between genes that are activated by LIN9 (i.e. that are downregulated after deletion of *Lin9*) and promoter binding of LIN9 (Figure 5F). In particular, LIN9 strongly bound to the promoters of cell cycle genes and E2F target genes (Figure 5G). While overall LIN9-binding correlated with expression changes, LIN9 only weakly bound to the promoters of some gene sets that are also downregulated in *Lin9* knockout hearts, including genes related to mitochondrial function, oxidative phosphorylation, metabolism, heart muscle contraction and ion channel activity (Figure 5G, Supplementary Figure S1D,E). Weak binding to the promoters of these genes

suggests that downregulation of these genes is an indirect consequence of loss of *Lin9*. Strikingly, when we evaluated the relationship between changes in gene expression upon cardiac-specific deletion of *Sav1* and LIN9-promoter occupancy, we found that promoters of genes activated in *Sav1* knockout hearts were also bound by LIN9 (Figure 5H). In contrast to LIN9 which bound to active promoters, ChIP-seq of YAP in E16.5 hearts showed that YAP predominantly binds to enhancers and super-enhancers rather than to promoters (Supplementary Figure S2A,B,C), which is consistent with recent genome wide studies in human cell lines (Galli *et al*, 2015; Stein *et al*, 2015; Pattschull *et al* 2019; Zanconato *et al*, 2015). Consequently, there was little overlap in the binding of YAP and LIN9 (Supplementary Figure S2B,C). This supports the idea that YAP does not regulate cell cycle promoters by directly binding to their promoters, but that YAP instead activates MMB-regulated cell cycle promoters from distant enhancers as previously shown in human MCF10A cells (Pattschull *et al*, 2019). In summary, the deletion of *Sav1* hyperactivates YAP, which in turn results in induction of cell cycle genes in a LIN9 dependent manner.

Lin9 is required for proliferation and mitosis of Hippo-deficient embryonic cardiomyocytes

We next examined the effect of MMB inactivation on proliferation of *Sav1* mutated cardiomyocytes. To assess proliferation, we stained E13.5 heart sections for the cell cycle marker Ki67. Cardiomyocytes were identified by co-staining for cardiac troponin T (cTnT). The proportion of Ki67-positive cardiomyocytes was significantly increased in Nkx2.5-Cre;Sav$^{fl/fl}$ hearts compared to control hearts with wildtype *Sav1*, indicating that loss of SAV1 promoted cardiomyocyte proliferation as has been reported previously (Figure 6A,B). The fraction of cardiomyocytes staining positive for phosphorylated histone H3 (pH3), a marker of mitotic cells, was also increased in *Nkx2.5-Cre;Sav1$^{fl/fl}$* hearts (Figure 6C,D). In contrast, proliferation and mitosis were strongly reduced by inactivation of *Lin9* and the increase in proliferation by *Sav1* deletion was blocked in *Sav1,Lin9* double mutant cardiomyocytes (Figure 6A-D). These

genetic experiments suggest that the proliferative phenotype due to the loss of the Hippo pathway member SAV1 is dependent on the MMB subunit LIN9.

We could not analyze the contribution of MMB to the Hippo-deficient phenotype at later embryonic or postnatal stages with this experimental system, because deletion of *Lin9* in heart progenitor cells by Nkx2.5-Cre resulted in embryonic lethality before embryonic day 18.5 (Supplementary Figure S3A). H&E stained embryonic heart sections showed that the thickness of the compact myocardium of both ventricles was reduced in *Lin9* knockout mice at E13.5 (Supplementary Figure S3B,C). Examination of H&E stained sections at higher magnification showed that nuclei in mutant cardiomyocytes were enlarged and pleomorphic (Supplementary Figure S3D,E). The reduced thickness of the myocardial walls and abnormal nuclear morphology in *Lin9* mutant hearts is consistent with the observed defects in cardiomyocyte proliferation and division and with the reduced expression of cell cycle genes (Supplementary Figure S1D,E).

Lin9 is required for proliferation of Hippo-deficient postnatal cardiomyocytes

To circumvent the embryonic lethality associated with deleting *Lin9* in early cardiac precursors, we used a transgenic mouse line with Cre recombinase driven by the alpha-MHC-promoter, which is active at a later stage during heart development compared to Nkx2.5-Cre (Agah *et al*, 1997). α-MHC-Cre; *Lin9*$^{fl/fl}$ mice survived into adulthood without any obvious heart phenotype and without differences in the heart to body weight when compared to heterozygous control animals (Figure 7A,B,C). The lack of a heart phenotype in α-MHC-Cre; *Lin9*$^{fl/fl}$ mice is not due to inefficient deletion of *Lin9* in the heart as revealed by combining with a mT/mG reporter strain (Muzumdar *et al*, 2007). Upon Cre-induced recombination of the mT/mG reporter gene, membrane bound Tomato (mT) is removed and the expression of membrane bound EGFP (mG) is activated (Figure 7D). FACS analysis revealed that recombination in the heart of α-MHC-Cre; *Lin9*$^{fl/fl}$ mice was almost 100% (Figure 7E,F).

Thus, while early cardiac deletion of *Lin9* in Nkx-Cre mice caused a dramatic and lethal phenotype, the complete deletion of *Lin9* at a later stage of development did not result in an

obvious phenotype, despite the fact that *Lin9* is expressed in the postnatal heart in wildtype mice (Supplementary Figure S4A,B). LIN9 also remained associated with the chromatin in postnatal hearts as determined by ChIP-seq (Figure 5E, Supplementary Figure S1C). The expression of the remaining MuvB core subunits also only modestly varied between the different developmental time points (Supplemental Figure S4A,B). Stronger changes in expression were observed with *Mybl2*, which declined at P1 compared to E16.5 and further decreased at P10, a pattern that was also confirmed on protein level (Supplemental Figure S4A,B). Correlating with a decreased expression of B-MYB, known mitotic target genes of MMB such as *Cenpf*, *Nusap1*, *Top2a* and *Birc5* were expressed at highest levels in embryonic hearts and strongly declined in P1 and P10 hearts (Supplemental Figure S4C,D). Conversely, *Mybl2* as well as a panel of mitotic MMB target genes were upregulated in *Sav1* knockout hearts (Supplemental Figure S4E). Together, these data indicate that the Hippo-pathway represses and MMB activates mitotic gene expression in cardiomyocytes.

To address whether LIN9 is required for mitosis of postnatal cardiomyocytes in Hippo-deficient hearts, we next crossed α-*MHC-Cre; Lin9*$^{fl/fl}$ mice to *Salv*$^{fl/fl}$ mice. Under normal conditions, there are almost no dividing cardiomyocytes in the postnatal heart, as expected. The deletion of *Sav1* robustly increased the fraction of mitotic cardiomyocytes, as has been shown previously (Figure 7G,H). Strikingly, this phenotype was suppressed when *Lin9* was lost and the fraction of mitotic cardiomyocytes remained low in α-MHC-Cre; *Sav1*$^{fl/fl}$*, Lin9*$^{fl/fl}$ double mutant mice, indicating a role for MMB in mitotic entry of postnatal cardiomyocytes due to Hippo deficiency.

Cardiomyocyte proliferation by activated YAP requires LIN9

To directly test whether increased cardiomyocyte proliferation due to activated YAP depends on MMB, we transduced cardiomyocytes with an adenovirus expressing a constitutive active version of YAP in which S127, the site of the inactivating phosphorylation by LATS kinases, is mutated to alanine (Figure 8A). To determine the requirement of MMB for YAP(S127A) induced proliferation, we used cardiomyocytes isolated from mice with a conditional allele of

Lin9 (*Lin9*$^{fl/fl}$) and expressing a hormone inducible CreER recombinase that can be activated by the addition of 4-hydroxytamoxifen (4-OHT). Treatment with 4-OHT resulted in efficient deletion of *Lin9 in* neonatal *Lin9*$^{fl/fl}$; CreER cardiomyocytes (Figure 8B). Expression of YAP(S127A) robustly induced mitotic entry of embryonic E14.5 and postnatal P1 cardiomyocytes, as reported before (Xin *et al*, 2011; Gise *et al*, 2012) (Figure 8C,D, Supplementary Figure S4A,B). Importantly, when *Lin9* was deleted by treatment with 4-OHT, the increase in pH3 positive cells by YAP(S127A) was strongly suppressed, indicating that YAP requires MMB to promote cardiomyocyte proliferation (Figure 8C,D, Supplementary Figure S5A,B). Importantly, the ability of YAP(S127A) to stimulate cardiomyocyte proliferation and to promote entry into mitosis was abolished by deletion of the YAP WW domains, which mediate the binding to MMB (Figure 8E,F, Supplementary Figure S5C,D). Similarly, a point mutant of YAPS127A deficient in binding to TEAD [YAP(S127A/S94A)], was also not able to increase proliferation and mitosis, indicating that these functions of YAP are TEAD dependent (Figure 8E,F, Supplementary Figure S5C,D).

We next asked whether proliferation of cardiomyocytes depends on the YAP-B-MYB interaction. We infected embryonal cardiomyocytes with an adenovirus expressing MY-COMP coupled to GFP through a T2A self-cleaving peptide. Infected cardiomyocytes were detected by their green fluorescence and by staining for cTnT (Supplementary Figure S5E). Staining for phospho-H3 showed that expression of MY-COMP strongly suppressed mitosis of embryonal cardiomyocytes (Figure 8G, Supplementary Figure S5E). Importantly, this effect was diminished by deletion of the PPXY motif in MY-COMP. Taken together these observations are consistent with the notion that YAP requires MMB to co-activate mitotic genes and promote mitotic entry of cardiomyocytes.

In another line of evidence, we investigated whether YAP is able to regulate MMB target genes in differentiated C2C12 myotubes. Co-immunoprecipitations confirmed that B-MYB and YAP interact in C2C12 myoblasts (Figure 8H). MMB target genes were expressed at high levels in asynchronous growing C2C12 cells and were downregulated during myogenic differentiation (Figure 8I). Expression of a constitutive active YAP(S127A) partially reverted the

downregulation of MMB target genes in differentiated cells (Figure 8I,J). Importantly, like the induction of proliferation of cardiomyocytes, the upregulation of MMB target genes by YAP was dependent on the WW and the TEAD-binding domains (Figure 8K). Strikingly activation of YAP target genes that are not regulated from distant enhancers but by binding of YAP to the proximal promoter, such as *Ctgf* and *Cyr61*, was independent of the WW domain. Taken together these data support the notion that YAP activates cell cycle genes from distant enhancers in a MMB dependent-manner.

DISCUSSION

One of the best characterized biological responses of YAP, the central downstream effector of the Hippo signaling pathway, is the induction of cell proliferation (Totaro *et al*, 2018). We have recently shown that the MMB complex is required for activation of G2/M genes by YAP (Pattschull *et al*, 2019). In this study we demonstrate a direct association between the MMB subunit B-MYB and YAP and we show that this interaction is of importance *in vivo* in for the development of the normal heart (Figure 8L).

The ability of B-MYB to bind to YAP is dependent on the tandem WW domains of YAP and a newly identified PPXY motif in B-MYB located in the central part of B-MYB between the DNA-binding domain and the transactivation domain. The YAP-binding domain of B-MYB does not overlap with the MuvB binding domain in the C-terminus of B-MYB that mediates binding of B-MYB to the MuvB core subunits LIN9 and LIN52 (Guiley *et al*, 2018). Therefore, the association of YAP with the MMB-complex is mediated by B-MYB.

Based on the binding studies we were able to create MY-COMP, a fragment of B-MYB containing the YAP binding domain of B-MYB. When fused to a nuclear localization signal and expressed in cells, MY-COMP interferes with the association of B-MYB and YAP, leading to multi- and binucleation in a PPXY dependent manner. Previous findings have defined key roles for the YAP WW domains in gene regulation, stimulation of proliferation and oncogenic transformation (Zhao *et al*, 2009). Our results suggest that at least parts of these effects are

mediated by the association of B-MYB with the WW domains. Targeting WW domain mediated interactions by MY-COMP, or by more potent inhibitors based on MY-COMP, may prove a valid strategy to inhibit the oncogenic pro-proliferative functions of YAP. Such inhibitors could serve as selective therapeutic target in cancers with high levels of YAP.

Recent studies have shown that the Hippo-YAP pathway plays essential roles during heart development and heart regeneration (Wang *et al*, 2018). While the deletion of YAP in embryonic heart impairs cardiomyocyte division, the expression of constitutively active YAP promotes cardiomyocyte proliferation (Gise *et al*, 2012; Xin *et al*, 2011; 2013; Del Re *et al*, 2013). We now show that MMB is required for the ability of YAP to induce cell division in this tissue. First, we used a mouse model in which cell cycle genes were induced in embryonic hearts by activation of YAP through the knockout of the Hippo pathway protein *Sav1*. These genes were not induced when the MuvB subunit *Lin9* was deleted together with *Sav1*. Proliferation of cardiomyocytes is also dependent on both MMB and YAP since deletion of *Lin9* abolishes the enhanced proliferation induced by deletion of *Sav1*. This requirement is not limited to the embryonic heart but the same dependency on *Lin9* for cardiomyocyte proliferation was also observed in postnatal hearts using *Lin9* / *Sav1* double knockout mice expressing the Cre transgene from the alpha-MHC promoter. Further evidence for this dependency on LIN9 comes from experiments using cultured embryonal or postnatal cardiomyocytes with a conditional *Lin9* allele and a hormone inducible Cre recombinase. Adenoviral expression of activated YAP was only able to induce mitosis when *Lin9* was present but not after Cre-mediated deletion of *Lin9*. Although it is possible that YAP and MMB could independently induce a similar set of genes required for cell cycle regulation, our findings that B-MYB and YAP directly interact, that the YAP induced cardiomyocyte proliferation depends on its WW domains and that cardiomyocyte mitosis is inhibited by MY-COMP, support the notion that the synergy is a result of the interaction between YAP and MMB.

Genome binding studies in embryonic hearts demonstrated that LIN9 binds to the promoters of cell cycle genes activated by YAP, indicating that these genes are direct targets of MMB. By ChIP-seq, YAP does not colocalize with LIN9 to the promoters of cell cycle genes but

instead binds to enhancers, consistent with recent data from human cancer cell lines where YAP also predominantly binds to distant sites (Zanconato *et al*, 2015; Stein *et al*, 2015; Galli *et al*, 2015). This suggests that YAP interacts with MMB-regulated promoters through chromatin looping, resulting in the activation of a subset of cell cycle genes, similar to what we have recently described for human MCF10A cells (Pattschull *et al*, 2019). Given that YAP not only interacts with MMB but that the MMB subunit B-MYB is also a transcriptional target of YAP, one can speculate that YAP and B-MYB form a positive feedback loop enabling expression of downstream cell cycle genes.

Remarkably, although LIN9 was required for cardiomyocyte cell cycle induction due to activated YAP, LIN9 was completely dispensable for homeostasis of the adult murine heart. This absence of a phenotype in adult cardiac-specific *Lin9* knockout mice was surprising, because LIN9 is a key subunit of the DREAM complex that is involved in repression of cell cycle genes in non-dividing cells (Sadasivam & DeCaprio, 2013). The observation that the genetic inactivation of *Lin9* in the postnatal heart is not associated with ectopic proliferation of cardiomyocytes suggests that loss of DREAM does not lead to de-repression of pro-proliferative genes. It is therefore possible that the main function of DREAM in cardiomyocytes is not to permanently silence cell cycle genes but to keep them in a poised state for re-activation by pro-proliferative signals. This notion is consistent with our finding that LIN9 remains associated with promoters of cell cycle genes in postnatal hearts and with the observation that DREAM binds in human cells to a nucleosome-free region at transcriptional start sites upstream from regions with high nucleosome density (Marceau *et al*, 2016). Further support from such a model comes from the observation that cell cycle promoters, as opposed to genes that regulate cell-cell contacts and the cytoskeleton, are readily accessible in adult murine hearts before introduction of a YAP5SA transgene (Monroe *et al*, 2019). Thus, LIN9 and DREAM may represent an epigenetic memory of a set of inactive but inducible cell cycle genes in postmitotic cardiomyocytes. It is therefore tempting to speculate that MuvB complexes play a dual role in cardiomyocyte proliferation, contributing to the inactive, but primed state of cell cycle genes as well as to their YAP-mediated activation. It will be important

to investigate whether epigenetic changes at MuvB bound promoters contribute to the loss of the regeneration capacity in adult hearts (Quaife-Ryan *et al*, 2017).

MATERIALS AND METHODS

Mice

Sav1$^{tm1.1Dupa}$/J mice were obtained from Jackson laboratories, in which LoxP sites flank exon 3 of the *Sav1* gene (Cai *et al*, 2010) . We have previously descripted *Lin9*^{fl} mice, in which LoxP sites flank exon 7 of the *Lin9* gene (Reichert *et al*, 2010). Cardiomyocyte-specific deletion of *Sav1* and *Lin9* was achieved by crossing mice to Nkx2.5-Cre mice (Stanley *et al*, 2002). Postnatal cardiomyocyte-specific deletion of *Sav1* and *Lin9* was achieved by crossing mice to α-MHC-Cre mice (Agah *et al*, 1997). To obtain Lin9$^{fl/fl}$CreER^{T2}, *Lin9*^{fl} mice were crossed with a mouse line ubiquitously expressing CreER^{T2} transgene (Hameyer *et al*, 2007). Mice were maintained in a C57/Bl6 background.

Cell culture

HEK293A (Thermo Fisher Scientific) cells, HeLa (ATCC® CCL-2™, female) cells and C2C12 (ATCC® CRL-1772™) cells were maintained in DMEM supplemented with 10% FCS (Thermo Fisher Scientific) and 1% penicillin/streptomycin (Thermo Fisher Scientific). Differentiation of C2C12 cells was induced by culturing in DMEM medium with 2 % horse serum (Sigma). Primary embryonic and postnatal cardiomyocytes were isolated by enzymatic digestion with the Pierce™ Primary cardiomyocyte isolation kit (Thermo Fisher Scientific). Cardiomyocytes were enriched by preplating on tissue-culture plastic to remove nonmyocytes. Cardiomyocytes were initially cultured for 48h on fibronectin-coated dishes with 5% horse serum (Sigma) and 1% penicillin/streptomycin (Thermo Fisher Scientific) and cardiomyocyte growth supplement at 37 °C and 5% CO2 to prevent proliferation of nonmyocytes. To induce the deletion of *Lin9*, conditional cardiomyocytes were treated with 100 nM 4-hydroxytamoxifen (Sigma) for 4 days.

Cardiomyocytes were transduced with adenovirus (multiplicity of infection, 25) in serum-free medium for 24 h and cultured for additional 48 h.

Adenovirus

Adenoviral constructs were constructed using the ViralPower adenoviral expression system (Thermo Fischer Scientific). Entry vectors containing YAPS127A, YAPS94AS127A and YAPS127AΔ155-263 were generated by PCR from p2xFLAG-CMV-YAPS127A (Komuro *et al*, 2003). Entry vectors containing GFP, HA-NLS-B-MYB (2-241)-T2A-GFP and HA-NLS-B-MYB (2-241, ΔPPXY)-T2A-GFP were generated by PCR from pCDNA4/TO-HA-NLS-SV40-B-MYB (this work) and pSpCas9n(BB)-2A-GFP (PX461) (Addgene #48140). All entry vectors were subcloned into pENTR3C (Invitrogen) and then recombined into pAd/CMV/V5-DEST using LR clonase II (Thermo Fischer Scientific). The production of YAP mutant and LacZ adenoviruses was performed in HEK293A cells according to the manufacturer's instructions. Adenoviruses were titered using the Adeno-X Rapid Titer Kit (TaKaRa).

RT-qPCR

Total RNA was isolated using peqGOLD TriFast (Peqlab) according to the manufacturer's instructions. RNA was transcribed using 100 units RevertAid reverse transcriptase (Thermo Fisher Scientific). Quantitative real–time PCR reagents were from Thermo Fisher Scientific and real-time PCR was performed using the Mx3000 (Stratagene) detection system. Primer sequences are listed in Supplementary Table 1. Expression differences were calculated as described before (Osterloh *et al*, 2007).

PLA

PLA was performed using the Duolink In Situ Kit (Sigma) according to the manufacturer's instructions. The following antibodies were used: LIN9 (Bethyl, A300-BL2981; 1:150), B-MYB phospho-T487 (ab76009; 1:100), YAP (Santa Cruz Biotechnology, sc-101199;1:200). For secondary staining, samples were incubated for 45 minutes with the following antibodies: cTnT

(DSHB; 1:50) or α-HA (Sigma, 1:200). After washing several times with buffer A, samples were incubated with for 20 minutes with secondary antibody: α-IgG2a conjugated to Alexa 488 (Thermo Fisher Scientific) and Hoechst 33258 (Sigma). Pictures were taken with an inverted Leica DMI 6000B microscope equipped with a Prior Lumen 200 fluorescence light source and a Leica DFC350 FX digital camera.

Plasmids

Expression vectors for truncated human FLAG-YAP constructs (aa 2-499, 2-287, 2-263, 2-154, 155-504, 264-504, 288-504 and Δ155-263) were constructed from pCMV-2xFLAG-YAP (Oka *et al*, 2008) by PCR. Expression vector for human GST-YAP constructs (aa 2-263, 155-263, 168-204, 231-263) were constructed by PCR in the pGEX-4-T2 vector. Truncated human HA-B-MYB constructs (aa 2-410, 2-331, 80-331, 80-410, 2-241, 2-79, 242-410) were generated from pCDNA4/TO-HA-B-MYB. Expression vector for truncated human 6xHis-B-MYB-2-241 and 2-241Δ198-201 (ΔPPXY) were constructed by PCR using appropriate oligonucleotides and were subcloned into pRSETA. Expression vectors containing HA-NLS-SV40-B-MYB-2-241, 2-79, 2-241 N174A(ΔDNA), 2-241 Δ198-201(ΔPPXY) were obtained by PCR and were subcloned into pCDNA4/TO vector.

Immunoblotting and immunoprecipitation

Whole protein extracts were obtained by lysing cells in TNN buffer (50mM Tris (pH 7.5), 120mM NaCl, 5mM EDTA, 0.5% NP40, 10mM $Na4P_2O_7$, 2mM Na_3VO_4, 100mM NaF, 1mM PMSF, 1mM DTT, 10mM β-glycerophosphate, protease inhibitor cocktail (Sigma)). Protein lysates or purified protein were separated by SDS-PAGE, transferred to a PVDF-membrane and detected by immunoblotting with the first and secondary antibodies: β-actin (Santa Cruz Biotechnology, sc-47778) 1:5000, B-MYB (clone LX015.1, (Tavner *et al*, 2007)) 1:5, anti-HA.11 (Covance, MMA-101P) 1:1000, anti-FLAG M2 (Sigma, F3165) 1:5000, anti-His (Sigma, H1029) 1:2000, Vinculin (Sigma, V9131) 1:10000, TOP2A (Santa Cruz Biotechnology, sc-365916) 1:1000, CDC20 (Santa Cruz Biotechnology, sc-5296) 1:500, YAP (Santa Cruz

Biotechnology, sc-10199) 1:1000, p-YAP(S127A) (Cell Signaling Technology, 4911) 1:1000, LIN9 (Bethyl, A300-BL2981), NUSAP1 (Geert Carmeliet) 1:1000, CENPF (Abcam, ab-5) 1:1000, anti-mouse-HRP (GE healthcare, NXA931) 1:5000 and HRP Protein A (BD Biosciences, 610438) 1:5000. For immunoprecipitation of FLAG-tagged proteins, protein G dynabeads (Thermo Fisher Scientific) were first coupled with 1 µg FLAG-antibody (Sigma, F3165) and then immunoprecipitated with 1mg whole cell lysate. After five times of washing with TNN, proteins were separated by SDS-PAGE and detected by immunoblotting using the desired antibodies.

Immunostaining

For immunostaining cardiomyocytes were seeded onto fibronectin coated coverslips. HeLa cells were seeded onto coverslips without fibronectin. Cells were fixed with 3% paraformaldehyde and 2% sucrose in PBS for 10 minutes at room temperature. Cells were permeabilized using 0.2% Triton X-100 (Sigma) in PBS for 5 minutes and blocked with 3% BSA in PBS-T (0.1% Triton X-100 in PBS) for 30 minutes. Primary antibodies were diluted in 3% BSA in PBS-T and incubated with the cells for 1 hour at room temperature. The following antibodies were used: TroponinT (CT3) (developmental studies hybridoma bank) 1:50, phospho-Histone H3 (Ser10) (Santa Cruz Biotechnology, sc-8656) 1:100, Ki-67 (SP6) (Thermo Scientific, RM-9106) 1:200, α-tubulin (B-5-1-2) (Santa Cruz Biotechnology, sc-23948) 1:150 and anti-HA (Sigma, H6908) 1:200. After three washing steps with PBS-T, secondary antibodies conjugated to Alexa 488 and 594 (Thermo Fisher Scientific) and Hoechst 33258 (Sigma) were diluted 1:500 in 3% BSA in PBS-T and incubated with the coverslips for 30 minutes at room temperature. Finally, slides were washed three times with PBS-T and mounted with Immu-Mount™ (Thermo Fisher Scientific). Pictures were taken with an inverted Leica DMI 6000B microscope equipped with a Prior Lumen 200 fluorescence light source and a Leica DFC350 FX digital camera.

Histology, H&E staining and immunohistochemistry

Freshly dissected embryos and postnatal hearts were fixed with bouin's fixative (picric acid (saturated; AppliChem), 10% (v/v) formaldehyde, 5% (v/v) (AppliChem) glacial acetic acid (Roth) embedded in paraffin and sectioned. Sections were deparaffinized, rehydrated and stained with hematoxylin and eosin or processed for immunostaining.

Following deparaffinization, antigen retrieval was performed by boiling samples in 10mM sodium citrate buffer (pH6.0) for 10 minutes in a microwave oven. After 30 minutes cool down, samples were blocked with 3% BSA in PBS-T (0.1% Tween-20 (AppliChem)) and incubated with the primary antibodies diluted in PBS-T over night at 4°C. The following antibodies were used: TroponinT (CT3) (developmental studies hybridoma bank) 1:50, phospho-Histone H3 (Ser10) (Santa Cruz Biotechnology, sc-8656) 1:100, Ki-67 (SP6) (Thermo Scientific, RM-9106) 1:200. After three washing steps with PBS-T, secondary antibodies conjugated to Alexa 488 and 594 (Thermo Fisher Scientific) and Hoechst 33258 (Sigma) were diluted 1:200 in 3% BSA in PBS-T and incubated with the coverslips for 2 hours at room temperature. Finally, slides were washed three times with PBS-T and mounted with Immu-Mount™ (Thermo Fisher Scientific). Pictures were taken with an inverted Leica DMI 6000B microscope equipped with a Prior Lumen 200 fluorescence light source and a Leica DFC350 FX digital camera.

Flow cytometry

Cardiomyocytes were isolated and enriched with the Pierce™ Primary cardiomyocyte isolation kit (Thermo Fisher Scientific) according to the manufacturer's instructions. Isolated and enriched cardiomyocytes were fixed with 4% PFA in PBS for 5 minutes. Detection was performed using a Beckman Coulter FC 500 cytomics and data were analyzed in CXP analysis 2.2 software. Gating and compensation were based on fluorophore-negative controls. 10.000 cells were analyzed per genotype.

RNA-Seq

For whole transcriptome analysis, total RNA was isolated in triplicates from ventricular heart tissue with the desired genotype. DNA libraries were generated using 1µg RNA with the

magnetic mRNA isolation module and NEBNext Ultra II RNA Library Prep Kit for Illumina (New England Biolabs). DNA library was amplified by 7 PCR cycles and quality was analyzed using the fragment analyzer (Advanced Analytical). Libraries were sequenced on the NextSeq 500 platform (Illumina).

ChIP-Seq

Chromatin was isolated from ventricular heart tissue of E16.5 or P10 hearts. In brief, minced tissue was fixed with 1% formaldehyde for 20 minutes at RT. The reaction was stopped by adding 125mM glycine for additional 5 minutes. Tissue was incubated in lysis buffer (50mM Tris-HCl pH8, 10mM EDTA, 1% SDS) for 1 hour at 4°C. Samples were sonicated for 1 minute at 25% amplitude (10s ON / 30s OFF) at 4°C, insoluble material was removed by centrifugation and chromatin was fragmented to an approximate size of 150 to 300bp by additional sonicating for 10 minutes at 25% amplitude (10 seconds On/ 30 seconds OFF) at 4°C using a Branson sonifier. Afterwards chromatin was diluted ten times in ChIP dilution buffer (50mM Tris-HCl pH8, 0.167M NaCl, 1.1% Triton X-100, 0.11% sodium deoxycholate). For immunoprecipitation, 9µg of the antibody was coupled to protein G dynabeads (Thermo Fisher Scientific) for 6 hours at 4°C and then incubated with fragmented chromatin over night at 4°C. Beads were washed in total twelve times with wash buffer I (50mM Tris-HCl pH8, 0.15M NaCl, 1mM EDTA, 0.1% SDS, 1% Triton X-100, 0.1% sodium deoxycholate), wash buffer II (50mM Tris-HCl pH8, 0.5M NaCl, 1mM EDTA, 0.1% SDS, 1% Triton X-100, 0.1% sodium deoxycholate), wash buffer III (50mM Tris-HCl pH8, 0.5M $LiCl_2$, 1mM EDTA, 1% Nonidet P-40, 0.7% sodium deoxycholate) and wash buffer IV (10mM Tris-HCl pH8, 1mM EDTA). 1mM PMSF and protease inhibitor cocktail were added freshly to all buffers. After washing chromatin was eluted in (10mM Tris-HCl pH8, 0.3M NaCl, 5mM EDTA, 0.5% SDS, 10µg/ml RNAseA) and crosslink was reversed at 65°C over night. Proteins were digested by adding 200µg/ml proteinase K at 55°C for 2 hours. DNA was purified using the QIAquick PCR Purification Kit (QIAGEN) and eluted in 50 µl EB buffer. Purified ChIP-DNA was quantified using the Quant-iT PicoGreen dsDNA Assay Kit (Thermo Fisher Scientific). DNA libraries were generated using 10ng purified ChIP-DNA

and the NEBNext®Ultra IIDNALibrary Prep Kit for Illumina® (New England Biolabs) according to the manufacturer's instructions. DNA library was amplified by 12-15 PCR cycles and quality was analyzed using the fragment analyzer (Advanced Analytical). Libraries were sequenced on the NextSeq 500 platform (Illumina). The following antibodies were used for ChIP-Seq: LIN9 (Bethyl, A300-BL2981), YAP (NB110-58358) and IgG from rabbit serum (Sigma, I5006).

GST-pulldown

Recombinant GST, GST-TEAD-WW1/2 (TEAD-binding domain and WW domain 1 and 2 of YAP fused to GST), GST-WW1/2-, GST-WW1, GST-WW2 or His-B-MYB(2-241) (amino acids 2-241 fused to 6 x his) were expressed in BL21 cells and purified on glutathione-linked sepharose beads (GE healthcare) or Ni-NTA-Agarose (GE healthcare, His-B-MYB). Lysates of HeLa cells expressing HA-tagged B-MYB constructs were incubated with 5 mg immobilized GST or GST-WW1/2-YAP for 3 hours at 4°C. Beads were washed six times with TNN buffer, resuspended in SDS protein sample buffer, boiled for 5 min, separated on a 10% SDS-PAGE gel, blotted and analyzed via immunoblotting.

Bioinformatic Analysis

After sequencing, bases were called using Illuminas GenerateFASTQ v1.1.0.64 software and sequencing quality was controlled with the FastQC script. For RNA-seq, reads were mapped with TopHat v2.1.0 (Kim *et al*, 2013) and BOWTIE2 (Langmead & Salzberg, 2012) with default parameters to the murine genome (mm10). Samples were normalized to the sample with the smallest number of mappable reads and a read count matrix for each Ensembl gene (GRCm38.p6) was generated with the *summarizeOverlaps* function in the R package {GenomicFeatures}. Before differential gene expression analysis, non- or weakly expressed genes were removed using the threshold: mean read count per gene over all samples >1. Differentially expressed genes were called with *EdgeR* and p-values were adjusted for multiple-testing with the Benjamini-Höchberg procedure (FDR: false discovery rate). Gene set

enrichment analyses were performed with signal2noise metric, 1000 permutations and a combined gene set database comprising Hallmark and C2 gene sets.

For ChIP-seq, sequenced reads were mapped to the *Mus musculus* genome mm10 with BOWTIE v1.2 (Langmead & Salzberg, 2012) with default parameters and subsequently normalized to the sample with the smallest number of sequenced reads. Peaks were called with MACS14 (Zhang *et al*, 2008) with maximal 3 duplicates, a p-value cut-off of 1e-5 and the input sample as control. Resulting peaks were annotated to the next transcriptional start of Ensembl genes with the *closestBed* function from the bedtools suite v2.26.0 (Quinlan & Hall, 2010). Overlapping peaks were identified with *bedtools intersect* and a minimal overlap of 1bp. LIN9 occupancy was calculated in a window of +/-1kb around TSSs with *bedtools coverage* function. Density matrices were generated with deeptools v2.3.5. (Ramírez *et al*, 2014) *computeMatrix* function at a resolution of 1bp and subsequently used for plotting heat maps with *plotHeatmap*. Mapped ChIP-seq data for histone marks were taken from the ENCODE portal (Sloan *et al*, 2016) (https://www.encodeproject.org/) with the following identifiers: ENCFF056JGV, ENCFF295HNV, ENCFF642EEK, ENCFF687BWU. Promoters, enhancers and super-enhancers were defined as described previously (Pattschull *et al*, 2019).

In box plots, the central line reflects the median, the borders of the boxes indicate the first and third quartile and whiskers extend to 1.5 of the interquartile range. Outliers are shown as dots. P-values were calculated with a two-tailed Wilcoxon rank sum test (unpaired samples) or Wilcoxons signed-rank test (paired samples).

ChIP- and RNA-sequencing datasets are available at the NCBI's Gene Expression Omnibus (Edgar *et al*, 2002) under the accession number GEO: GSE137132.

ACKNOWLEDGEMENTS

We thank Stefanie Hauser and Grit Weinstock for critical reading of the manuscript. This work was supported by grants from the Deutsche Krebshilfe (70113138) and Deutsche Forschungsgemeinschaft, DFG (GA575/9-1) towards SG.

AUTHOR CONTRIBUTIONS

S.G. and M.G. planned the study and designed the experiments. M.G., L.H., M.S., K.M.W. and S.P. conducted the experiments. M.G. and S.G. analyzed the data. S.W. performed the bioinformatic analyses. C.P.A. performed next-generation sequencing. S.G. and M.G. wrote the manuscript.

CONFLICT OF INTEREST

The authors declare that they have no conflict of interest.

REFERENCES

Agah R, Frenkel PA, French BA, Michael LH, Overbeek PA & Schneider MD (1997) Gene recombination in postmitotic cells. Targeted expression of Cre recombinase provokes cardiac-restricted, site-specific rearrangement in adult ventricular muscle in vivo. *J Clin Invest* **100:** 169–179

Cai J, Zhang N, Zheng Y, de Wilde RF, Maitra A & Pan D (2010) The Hippo signaling pathway restricts the oncogenic potential of an intestinal regeneration program. *Genes Dev* **24:** 2383–2388

Chen HI & Sudol M (1995) The WW domain of Yes-associated protein binds a proline-rich ligand that differs from the consensus established for Src homology 3-binding modules. *Proc Natl Acad Sci USA* **92:** 7819–7823

Del Re DP, Yang Y, Nakano N, Cho J, Zhai P, Yamamoto T, Zhang N, Yabuta N, Nojima H, Pan D & Sadoshima J (2013) Yes-associated protein isoform 1 (Yap1) promotes cardiomyocyte survival and growth to protect against myocardial ischemic injury. *J Biol Chem* **288:** 3977–3988

Edgar R, Domrachev M & Lash AE (2002) Gene Expression Omnibus: NCBI gene expression and hybridization array data repository. *Nucleic Acids Res* **30:** 207–210

Fischer M & Müller GA (2017) Cell cycle transcription control: DREAM/MuvB and RB-E2F complexes. *Crit. Rev. Biochem. Mol. Biol.***:** 1–25

Galli GG, Carrara M, Yuan W-C, Valdes-Quezada C, Gurung B, Pepe-Mooney B, Zhang T, Geeven G, Gray NS, de Laat W, Calogero RA & Camargo FD (2015) YAP Drives Growth by Controlling Transcriptional Pause Release from Dynamic Enhancers. *Mol Cell* **60:** 328–337

Gise von A, Lin Z, Schlegelmilch K, Honor LB, Pan GM, Buck JN, Ma Q, Ishiwata T, Zhou B, Camargo FD & Pu WT (2012) YAP1, the nuclear target of Hippo signaling, stimulates heart growth through cardiomyocyte proliferation but not hypertrophy. *Proc Natl Acad Sci USA* **109:** 2394–2399

Guiley KZ, Iness AN, Saini S, Tripathi S, Lipsick JS, Litovchick L & Rubin SM (2018) Structural mechanism of Myb-MuvB assembly. *Proc Natl Acad Sci USA* **115:** 10016–10021

Guiley KZ, Liban TJ, Felthousen JG, Ramanan P, Litovchick L & Rubin SM (2015) Structural mechanisms of DREAM complex assembly and regulation. *Genes Dev* **29:** 961–974

Hameyer D, Loonstra A, Eshkind L, Schmitt S, Antunes C, Groen A, Bindels E, Jonkers J, Krimpenfort P, Meuwissen R, Rijswijk L, Bex A, Berns A & Bockamp E (2007) Toxicity of ligand-dependent Cre recombinases and generation of a conditional Cre deleter mouse allowing mosaic recombination in peripheral tissues. *Physiol. Genomics* **31:** 32–41

Heallen T, Morikawa Y, Leach J, Tao G, Willerson JT, Johnson RL & Martin JF (2013) Hippo signaling impedes adult heart regeneration. *Development* **140:** 4683–4690

Heallen T, Zhang M, Wang J, Bonilla-Claudio M, Klysik E, Johnson RL & Martin JF (2011) Hippo pathway inhibits Wnt signaling to restrain cardiomyocyte proliferation and heart size. *Science* **332:** 458–461

Hong W & Guan K-L (2012) The YAP and TAZ transcription co-activators: key downstream effectors of the mammalian Hippo pathway. *Seminars in cell & developmental biology* **23:** 785–793

Kim D, Pertea G, Trapnell C, Pimentel H, Kelley R & Salzberg SL (2013) TopHat2: accurate alignment of transcriptomes in the presence of insertions, deletions and gene fusions. *Genome Biol* **14:** R36

Komuro A, Nagai M, Navin NE & Sudol M (2003) WW domain-containing protein YAP associates with ErbB-4 and acts as a co-transcriptional activator for the carboxyl-terminal fragment of ErbB-4 that translocates to the nucleus. *J Biol Chem* **278:** 33334–33341

Langmead B & Salzberg SL (2012) Fast gapped-read alignment with Bowtie 2. *Nat. Methods* **9:** 357–359

Leach JP, Heallen T, Zhang M, Rahmani M, Morikawa Y, Hill MC, Segura A, Willerson JT & Martin JF (2017) Hippo pathway deficiency reverses systolic heart failure after infarction. *Nature* **550:** 260–264

Lin Z, Gise von A, Zhou P, Gu F, Ma Q, Jiang J, Yau AL, Buck JN, Gouin KA, van Gorp PRR, Zhou B, Chen J, Seidman JG, Wang D-Z & Pu WT (2014) Cardiac-specific YAP activation improves cardiac function and survival in an experimental murine MI model. *Circ. Res.* **115:** 354–363

Litovchick L, Sadasivam S, Florens L, Zhu X, Swanson SK, Velmurugan S, Chen R, Washburn MP, Liu XS & DeCaprio JA (2007) Evolutionarily conserved multisubunit RBL2/p130 and E2F4 protein complex represses human cell cycle-dependent genes in quiescence. *Mol Cell* **26:** 539–551

Liu S & Martin JF (2019) The regulation and function of the Hippo pathway in heart regeneration. *Wiley Interdiscip Rev Dev Biol* **8:** e335

Macias MJ, Martin-Malpartida P & Massagué J (2015) Structural determinants of Smad function in TGF-β signaling. *Trends Biochem Sci* **40:** 296–308

Marceau AH, Felthousen JG, Goetsch PD, Iness AN, Lee H-W, Tripathi SM, Strome S, Litovchick L & Rubin SM (2016) Structural basis for LIN54 recognition of CHR elements in cell cycle-regulated promoters. *Nat Commun* **7:** 12301

Meng Z, Moroishi T & Guan K-L (2016) Mechanisms of Hippo pathway regulation. *Genes Dev* **30:** 1–17

Monroe TO, Hill MC, Morikawa Y, Leach JP, Heallen T, Cao S, Krijger PHL, de Laat W, Wehrens XHT, Rodney GG & Martin JF (2019) YAP Partially Reprograms Chromatin Accessibility to Directly Induce Adult Cardiogenesis In Vivo. *Dev Cell* **48:** 765–779.e7

Morikawa Y, Zhang M, Heallen T, Leach J, Tao G, Xiao Y, Bai Y, Li W, Willerson JT & Martin JF (2015) Actin cytoskeletal remodeling with protrusion formation is essential for heart regeneration in Hippo-deficient mice. *Science signaling* **8:** ra41–ra41

Muzumdar MD, Tasic B, Miyamichi K, Li L & Luo L (2007) A global double-fluorescent Cre reporter mouse. *Genesis* **45:** 593–605

Oka T, Mazack V & Sudol M (2008) Mst2 and Lats kinases regulate apoptotic function of Yes kinase-associated protein (YAP). *J Biol Chem* **283:** 27534–27546

Osterloh L, Eyss von B, Schmit F, Rein L, Hübner D, Samans B, Hauser S & Gaubatz S (2007) The human synMuv-like protein LIN-9 is required for transcription of G2/M genes and for entry into mitosis. *EMBO J* **26:** 144–157

Pattschull G, Walz S, Gründl M, Schwab M, Rühl E, Baluapuri A, Cindric-Vranesic A, Kneitz S, Wolf E, Ade CP, Rosenwald A, Eyss von B & Gaubatz S (2019) The Myb-MuvB Complex Is Required for YAP-Dependent Transcription of Mitotic Genes. *Cell Rep* **27:** 3533–3546.e7

Pilkinton M, Sandoval R & Colamonici OR (2007) Mammalian Mip/LIN-9 interacts with either the p107, p130/E2F4 repressor complex or B-Myb in a cell cycle-phase-dependent context distinct from the Drosophila dREAM complex. *Oncogene* **26:** 7535–7543

Quaife-Ryan GA, Sim CB, Ziemann M, Kaspi A, Rafehi H, Ramialison M, El-Osta A, Hudson JE & Porrello ER (2017) Multicellular Transcriptional Analysis of Mammalian Heart Regeneration. *Circulation* **136:** 1123–1139

Quinlan AR & Hall IM (2010) BEDTools: a flexible suite of utilities for comparing genomic features. *Bioinformatics* **26:** 841–842

Ramírez F, Dündar F, Diehl S, Grüning BA & Manke T (2014) deepTools: a flexible platform for exploring deep-sequencing data. *Nucleic Acids Res* **42:** W187–91

Reichert N, Wurster S, Ulrich T, Schmitt K, Hauser S, Probst L, Götz R, Ceteci F, Moll R, Rapp U & Gaubatz S (2010) Lin9, a subunit of the mammalian DREAM complex, is essential for embryonic development, for survival of adult mice, and for tumor suppression. *Mol Cell Biol* **30:** 2896–2908

Sadasivam S & DeCaprio JA (2013) The DREAM complex: master coordinator of cell cycle-dependent gene expression. *Nat Rev Cancer* **13:** 585–595

Sadasivam S, Duan S & DeCaprio JA (2012) The MuvB complex sequentially recruits B-Myb and FoxM1 to promote mitotic gene expression. *Genes Dev* **26:** 474–489

Schmit F, Korenjak M, Mannefeld M, Schmitt K, Franke C, Eyss von B, Gagrica S, Hänel F, Brehm A & Gaubatz S (2007) LINC, a human complex that is related to pRB-containing complexes in invertebrates regulates the expression of G2/M genes. *Cell Cycle* **6:** 1903–1913

Sloan CA, Chan ET, Davidson JM, Malladi VS, Strattan JS, Hitz BC, Gabdank I, Narayanan AK, Ho M, Lee BT, Rowe LD, Dreszer TR, Roe G, Podduturi NR, Tanaka F, Hong EL & Cherry JM (2016) ENCODE data at the ENCODE portal. *Nucleic Acids Res* **44:** D726–32

Stanley EG, Biben C, Elefanty A, Barnett L, Koentgen F, Robb L & Harvey RP (2002) Efficient Cre-mediated deletion in cardiac progenitor cells conferred by a 3'UTR-ires-Cre allele of the homeobox gene Nkx2-5. *Int. J. Dev. Biol.* **46:** 431–439

Stein C, Bardet AF, Roma G, Bergling S, Clay I, Ruchti A, Agarinis C, Schmelzle T, Bouwmeester T, Schübeler D & Bauer A (2015) YAP1 Exerts Its Transcriptional Control via TEAD-Mediated Activation of Enhancers. *PLoS Genet* **11:** e1005465

Tavner F, Frampton J & Watson RJ (2007) Targeting an E2F site in the mouse genome prevents promoter silencing in quiescent and post-mitotic cells. *Oncogene* **26:** 2727–2735

Totaro A, Panciera T & Piccolo S (2018) YAP/TAZ upstream signals and downstream responses. *Nat Cell Biol* **20:** 888–899

Wang J, Liu S, Heallen T & Martin JF (2018) The Hippo pathway in the heart: pivotal roles in development, disease, and regeneration. *Nat Rev Cardiol* **15:** 672–684

Werwein E, Schmedt T, Hoffmann H, Usadel C, Obermann N, Singer JD & Klempnauer K-H (2012) B-Myb promotes S-phase independently of its sequence-specific DNA binding activity and interacts with polymerase delta-interacting protein 1 (Pdip1). *Cell Cycle* **11:** 4047–4058

Xin M, Kim Y, Sutherland LB, Murakami M, Qi X, McAnally J, Porrello ER, Mahmoud AI, Tan W, Shelton JM, Richardson JA, Sadek HA, Bassel-Duby R & Olson EN (2013) Hippo pathway effector Yap promotes cardiac regeneration. *Proc Natl Acad Sci USA* **110:** 13839–13844

Xin M, Kim Y, Sutherland LB, Qi X, McAnally J, Schwartz RJ, Richardson JA, Bassel-Duby R & Olson EN (2011) Regulation of insulin-like growth factor signaling by Yap governs cardiomyocyte proliferation and embryonic heart size. *Science signaling* **4:** ra70

Zanconato F, Forcato M, Battilana G, Azzolin L, Quaranta E, Bodega B, Rosato A, Bicciato S, Cordenonsi M & Piccolo S (2015) Genome-wide association between YAP/TAZ/TEAD and AP-1 at enhancers drives oncogenic growth. *Nat Cell Biol* **17:** 1218–1227

Zhang Y, Liu T, Meyer CA, Eeckhoute J, Johnson DS, Bernstein BE, Nusbaum C, Myers RM, Brown M, Li W & Liu XS (2008) Model-based analysis of ChIP-Seq (MACS). *Genome Biol* **9:** R137

Zhao B, Kim J, Ye X, Lai Z-C & Guan K-L (2009) Both TEAD-binding and WW domains are required for the growth stimulation and oncogenic transformation activity of yes-associated protein. *Cancer Res* **69:** 1089–1098

FIGURE LEGENDS

Figure 1: Interaction between MMB and the Hippo coactivator YAP A) Scheme of YAP deletion mutants used in co-immunoprecipitation experiments. B) Co-immunoprecipitation of ectopically expressed HA-B-MYB with flag-tagged YAP. Lysates of HeLa cells expressing HA-B-MYB and flag-YAP mutants (see A) were immunoprecipitated with flag-antiserum and immunoblotted with an anti-HA-antibody. 3 % percent of total lysate was immunoblotted (Input). C) Densiometric quantification of binding data shown in B using ImageJ. Binding is relative to HA-B-MYB control cells. n=3 biological replicates. D) Co-immunoprecipitation between flag-YAP and HA-B-MYB demonstrating that the WW domains of YAP are required for the interaction with B-MYB. E) Scheme of the GST fusion constructs used in pulldown experiments. F) Pulldown experiments with 5 µg of the indicated recombinant GST-fusion proteins and with HA-B-MYB, HA-TEAD4 and HA-EB1 expressed in HeLa cells. Bound proteins were detected with an anti-HA antibody. HA-TEAD was used as a positive control for the interaction with GST-YAP-TEAD-WW1/2 and HA-EB1 served as a negative control. A coomassie brilliant blue stained gel of the purified proteins is shown at the bottom. G) Pulldown experiments of the indicated GST fusion proteins with HA-B-MYB. Bound B-MYB was detected by immunoblotting with an HA-antibody. Input: 3 % of the lysate used for the pulldown was loaded onto the gel. Actin served as a control. Ponceau staining was used to detect the recombinant GST-proteins.

Figure 2: A PPXY motif is involved in binding of B-MYB to YAP A) Scheme of the domain structure of B-MYB and of the deletion constructs used in pulldown experiments. B) Pulldown experiments with GST-WW1 and HA-tagged B-MYB constructs expressed in HeLa cells. Bound proteins were detected by immunoblotting with a HA antibody. Input: 3 % of the lysate used for the pulldown was loaded onto the gel. Vinculin was used as a control. Ponceau staining was used to detect the recombinant GST-proteins. C) Pulldown experiments with the indicated GST-fusion proteins and with recombinant, purified his-tagged B-MYB(2-241). Recombinant proteins were detected by Ponceau S staining (left). Bound his-tagged B-MYB(2-

241) was detected by western-blotting with an anti-his antibody (right). D) Pulldown experiments with GST-WW and his-tagged B-MYB(2-241) and B-MYB(2-241,ΔPPXY). Bound B-MYB was detected with a his-antibody. Input: 3 % of the recombinant his-tagged B-MYB constructs were loaded onto the gel. Recombinant proteins were detected by Ponceau S staining. E) Co-immunoprecipitation experiments of the indicated B-MYB constructs with flag-YAP. Lysates of HeLa cells expressing flag-YAP and HA-B-MYB (wt and ΔPPXY) were immunoprecipitated with flag-antiserum and immunoblotted with an anti-HA-antibody and anti-flag antibody. 3 % percent of total lysate was immunoblotted (Input). F) Densiometric quantification of the binding of HA-MYB and HA-B-MYBΔPPXY to flag-YAP using Image J. Binding is relative to HA-B-MYB control cells. Error bars show SEMs of biological replicates (n=3). Student's t-test **= $p<0.01$

Figure 3: Expression of MY-COMP, the YAP-binding domain of B-MYB, disrupts the association between B-MYB and YAP and leads to errors in cell division A) Scheme for the disruption of the YAP-B-MYB interaction by expression of the YAP-binding domain of B-MYB fused to an NLS (YBD). B) HeLa cells were transfected with flag-YAP, HA-B-MYB and MY-COMP (HA-NLS-B-MYB(2-241)) as indicated. Flag-YAP was immunoprecipitation and bound HA-B-MYB was detected by immunoblotting. When MY-COMP was cotransfected, the interaction between flag-YAP and HA-B-MYB was decreased. Input: 3 % of the lysate was loaded onto the gel. C) Densiometric quantification of the binding of HA-B-MYB to flag-YAP in presence and absence of MY-COMP using Image J. Binding is relative to FLAG-YAP control cells. N=3 biological replicates. D) Proximity ligation assay (PLA) of endogenous YAP and B-MYB upon transfection of MY-COMP. Cell expressing MY-COMP were identified by HA staining (green) . E) Quantification of the proximity ligation assay shown in D. Student's t-test. F) Expression of the indicated HA-NLS-B-MYB constructs was verified by immunoblotting with an HA-antibody. The expression of the indicated HA-tagged B-MYB constructs did not affect the expression of endogenous B-MYB, YAP and YAP phosphorylated on S127 (p-YAP) as determined by immunoblotting. Actin served as a control. G) Microphotographs showing

examples of the different phenotypes following expression of MY-COMP. Bar: 25 µm. H) Quantification of the fraction of binucleated and multinucleated cells and cells with micronuclei following expression of the indicated HA-B-MYB constructs. N=4 biological replicates. C), E), H): Error bars indicate SEMs. Student's t-test. *=p<0.05, *=p<0.01, ***=p<0.001, ns= not significant.

Figure 4: Interaction between YAP and MMB in cardiomyocytes A) Proximity ligation assays (PLA) showing that YAP and LIN9 and YAP and B-MYB interact in the nuclei of E14.5 cardiomyocytes. siRNA mediated depletion of YAP/TAZ, LIN9 or B-MYB served as control. Interactions are indicated by red fluorescent dots. Cardiomyocytes were identified by immunostaining for cTnT (green). Bar: 25 µm B) PLA assays shown in A were quantified by counting the number of interactions per nucleus.

Figure 5: Cell cycle genes upregulated in Sav1 knockout hearts are direct targets of LIN9 A) GSEA comparing the effect of deletion of Sav1 in Nkx-Cre LIN9 wt and LIN9 KO heart ventricles at E13.5. The C2 MSigDB was spiked with the Hallmark gene sets. Gene sets related to cell cycle are highlighted in blue. NES: normalized enrichment score. B) Boxplot comparing differences in E2F target gene expression taken from the MSigDB Hallmark collection between Nkx-Cre; $Sav1^{fl/fl}$ (Sav1 KO) and Nkx-Cre; $Sav1^{+/+}$ (Sav1 wt) heart ventricles in $LIN9^{fl/fl}$ (LIN9 KO) or $Lin9^{fl/+}$ (LIN9 wt) background. p-values were calculated using an unpaired, two-tailed Wilcoxon test and outliers are not shown. C) Expression of the indicated genes relative to actin and *Hprt* in heart ventricles of embryos with the indicated genotypes was analyzed by RT-qPCR. D) Histogram showing the absolute distance between overlapping LIN9 peaks called in E16.5 and P10 heart ventricles located in promoters (n=1,458) at a resolution of 20 bp. E) Bar plot illustrating the genomic localization of LIN9 in fetal (E16.5) and postnatal (P10) heart ventricles. Active promoters, enhancers and super-enhancers are defined based on publicly available ChIP-seq data for histone marks reported in GSE31039. F) Bin plot correlating changes in gene expression in Nkx-Cre; $Lin9^{fl/fl}$ heart ventricles with binding of LIN9 to the

promoter. Analyzed was a region 1kb upstream the TSS and input signals were subtracted. 15,642 expressed genes were grouped into 15 bins and the mean of each bin is plotted. The dashed line reflects a regression based on a linear model. G) Boxplot depicting LIN9 binding at genes from the gene sets shown in Supplementary Figure S1E. Analyzed was a region of +/-250bp around the TSS and p-values were calculated using a paired two-tailed Wilcoxon test. H) Bin plot correlating changes in gene expression after *Sav1* knockout in Nkx-Cre hearts with binding of LIN9 to the promoters at E16.5. Analyzed was a region 1kb upstream the TSS and input signals were subtracted. 15,642 expressed genes were grouped into 15 bins and the mean of each bin is plotted. The dashed line reflects a regression based on a linear model.

Figure 6: Proliferation and mitosis of embryonic cardiomyocytes following Hippo inactivation depends on LIN9. A) and B) Heart sections from E13.5 mice with the indicated genotypes were stained for the proliferation marker Ki67 (red). Cardiomyocytes were identified by staining for cTnT (green). Example microphotographs are shown in (A), the quantification of Ki67-positive cells is shown in (B). Scale bar: 25µm. Error bars indicate SDs. Number of mice analyzed per genotype: $Lin9^{fl/+};Sav1^{fl/+}$ n=5, $Lin9^{fl/+};Sav1^{fl/fl}$ n=4, $Lin9^{fl/fl};Sav1^{fl/+}$ n=6 and $Lin9^{fl/fl};Sav1^{fl/fl}$ n=5 C) and D) Heart sections from E13.5 mice with the indicated genotypes were stained for the mitosis marker pH3 (red). Cardiomyocytes were identified by staining for cTnT (green). Example microphotographs are shown in (C), the quantification of pH3-positive cells is shown in (D). Number of mice analyzed per genotype: $Lin9^{fl/+};Sav1^{fl/+}$ n=5, $Lin9^{fl/+};Sav1^{fl/fl}$ n=4, $Lin9^{fl/fl};Sav1^{fl/+}$ n=6 and $Lin9^{fl/fl};Sav1^{fl/fl}$ n=6. Error bars indicate SD. C, E: Student's t-test. *=p<0.05, *=p<0.01, ***=p<0.001, ns= not significant.

Figure 7: LIN9 is required for cardiomyocyte proliferation in Hippo-deficient, postnatal hearts A) Breeding scheme and resulting genotypes. Number of mice with the indicated genotypes at P10 and P21-25. B) H&E-stained sections of hearts from α-MHC-Cre;$Lin9^{fl/+}$ and α-MHC-Cre;$Lin9^{fl/fl}$ mice at P10. Scale bar: 1000µm C) heart to body weight of α-MHC-Cre;$Lin9^{fl/+}$ and α-MHC-Cre;$Lin9^{fl/fl}$ mice at p10. n= 14 control mice and n=9 $Lin9^{fl/fl}$ mice. Error bars

indicate SEM. Student's t-test. D) Scheme of the mT/mG reporter. Upon expression of Cre-recombinase, mTomato is deleted and mGFP is activated. E) FACS analysis of mTomato and mEGFP positive cardiomyoyctes derived from hearts of E13.5 and P10 hearts with the indicated genotypes. F) Quantification of mTomato (mT) and mEGFP (mG) positive cardiomyoyctes. Number of mice analyzed per genotype: E13.5 *Lin9*$^{fl/+}$ n=4; E13.5 *Lin9*$^{fl/fl}$ n=4; P10 *Lin9*$^{fl/+}$ n=3; P10 *Lin9*$^{fl/fl}$ n=3. G) and H) The fraction of pH3-positive cardiomyocytes in the hearts of 10 days old mice with the indicated genotypes was determined by immunostaining. Cardiomyocytes were identified by staining for cTnT. Scale bar 25µm. Number of mice analyzed per genotype: *Lin9*$^{fl/+}$;*Sav1*$^{fl/+}$ n=3, *Lin9*$^{fl/+}$;*Sav1*$^{fl/fl}$ n=6, *Lin9*$^{fl/fl}$;*Sav1*$^{fl/+}$ n=3 and *Lin9f*$^{l/fl}$;*Sav1*$^{fl/fl}$ n=7. F), H): Error bars indicate SDs. Student's t-test. *=p<0.05, *=p<0.01, ***=p<0.001, ns= not significant

Figure 8: Cardiomyocyte proliferation by activated YAP requires MMB A) Cardiomyocytes isolated from neonatal (P1) *Lin9*$^{fl/fl}$;CreER mice were transduced with a LacZ control (Ade-LacZ) or FLAG-YAP(S127A) expressing adenovirus. Expression of YAPS127A was verified by immunoblotting with a flag-antibody 72 hours after adenoviral transduction. Actin served as a control. B) Cardiomyocytes isolated from *Lin9*$^{fl/fl}$;CreER hearts were treated without and with 4-OHT as indicated and the deletion of *Lin9* was verified by genomic PCR. C) and D) Embryonal (E14.5) *Lin9*$^{fl/fl}$;CreER cardiomyocytes (C) or postnatal (P1) cardiomyocytes (D) were transduced with Ade-LacZ or with Ade-YAP(S127A) and treated with or without 4-OHT. The fraction of pH3-positive cardiomyocytes was quantified. Error bars show SDs of biological replicates (n=3). E) and F) Cardiomyocytes were transduced with Ade-LacZ, Ade-YAP(S127A), and Ade-YAP(S127A/S94A) or with Ade-YAP(S127A/ΔWW). The fraction of pH3-positive positive (E) and Ki67 (F) cardiomyocytes was determined. Error bars show SD. (E) n=6-8, (F) n=3-4 biological replicates. G) Disruption of the YAP-B-MYB interaction by MY-COMP inhibits mitosis of cardiomyocytes. Embryonal cardiomyocytes were infected with adenoviruses expressing GFP, HA-NLS-B-MYB(2-241) coupled to GFP through a T2A self-cleaving peptide or with HA-NLS-B-MYB(2-241,ΔPPXY) coupled to GFP through a T2A self-

cleaving peptide. Infected cardiomyocytes were detected by staining for cTnT and by their green fluorescence. Mitotic cells were quantified by staining for phospho-H3. Example microphotographs are provided in Supplementary Figure S5. H) Co-immunoprecipitation of ectopically expressed flag-YAP and HA-B-MYB demonstrating the interaction between YAP and B-MYB in C2C12 cells. IP, immunoprecipitation. Input: 3% of the amount used for IP was loaded on the gel. I) Undifferentiated C2C12 myoblasts (undiff) or differentiated C2C12 myotubes (diff) were infected with Ade-LacZ or Ade-YAP(S127A). After 2 days, the expression of the indicated proteins was analyzed by immunoblotting. Actin served as a loading control. J) and K) Differentiated C2C12 myotubes were infected with the indicated adenoviral expression constructs. J) The expression of the YAP constructs was analyzed by immunoblotting with a flag-antibody. Actin served as a loading control. K) mRNA expression of the indicated genes relative to *Actin* and *Hprt* was analyzed by RT-qPCR. Error bars show SD of technical triplicates from one representative experiment (n=3). L) Model summarizing the results. See text for details. C, D, E, F, G: Student's t-test. *=p<0.05 **=p<0.01 ***=p<0.001.

Figure 1

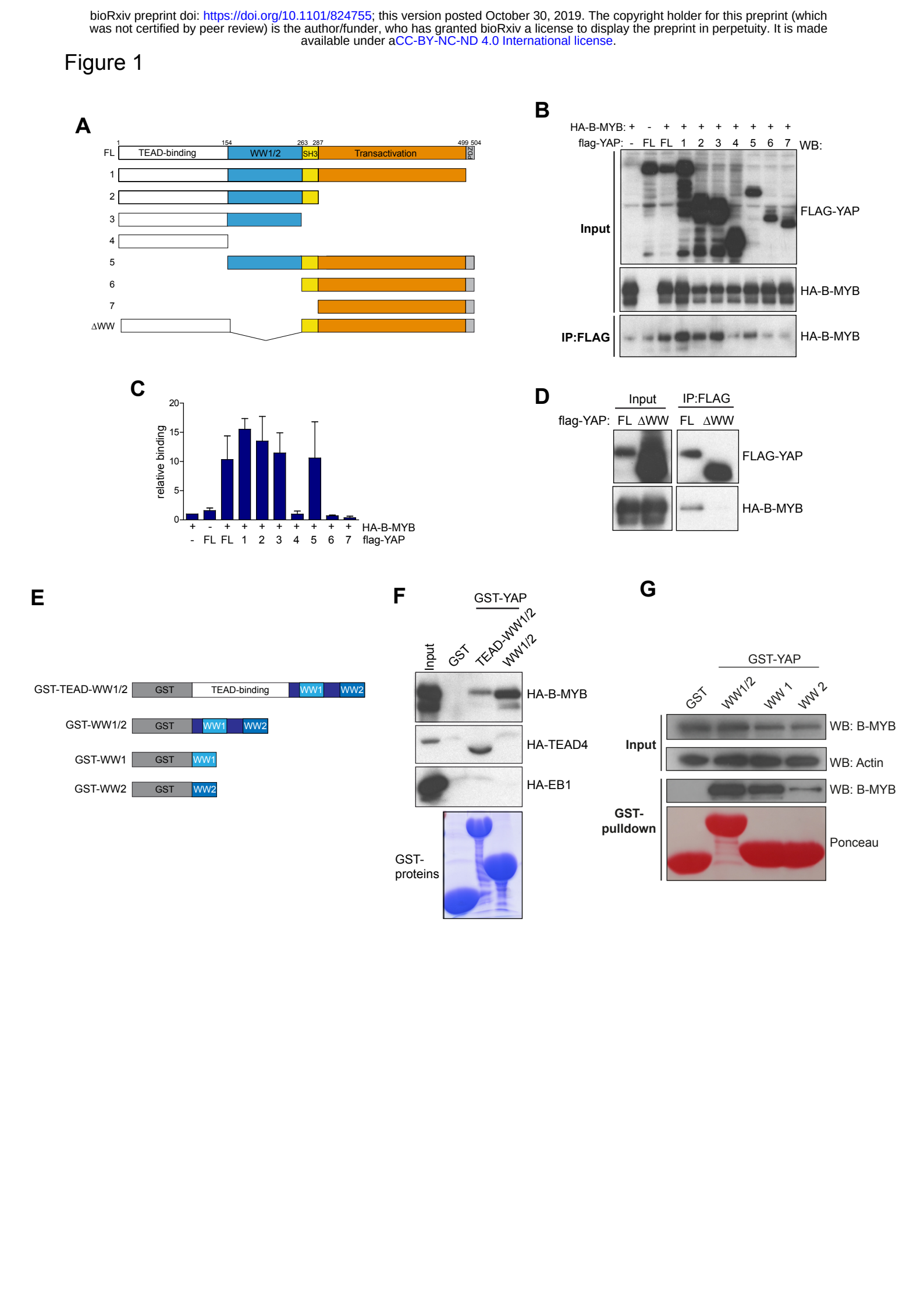

Figure 2

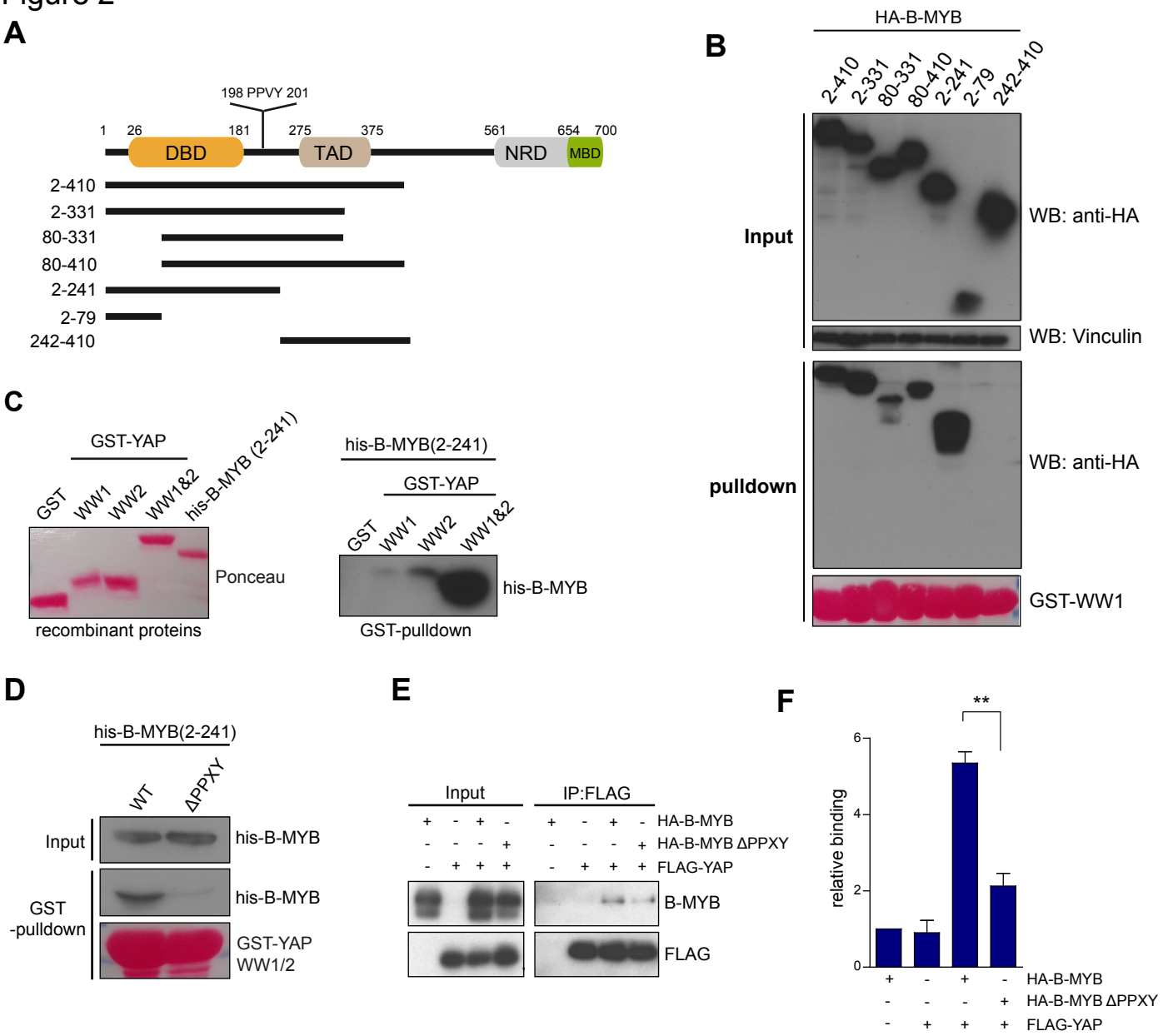

Figure 3

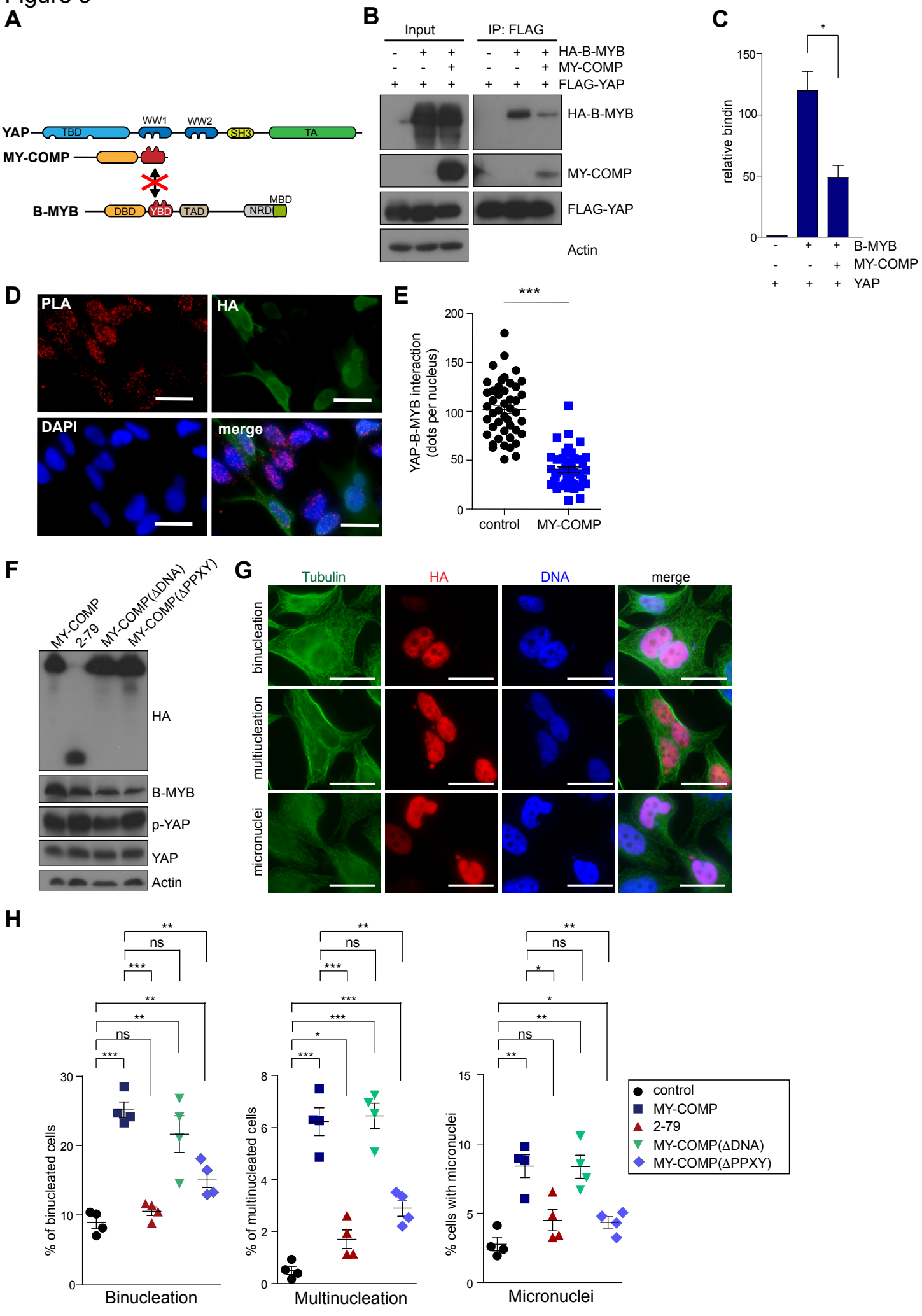

Figure 4

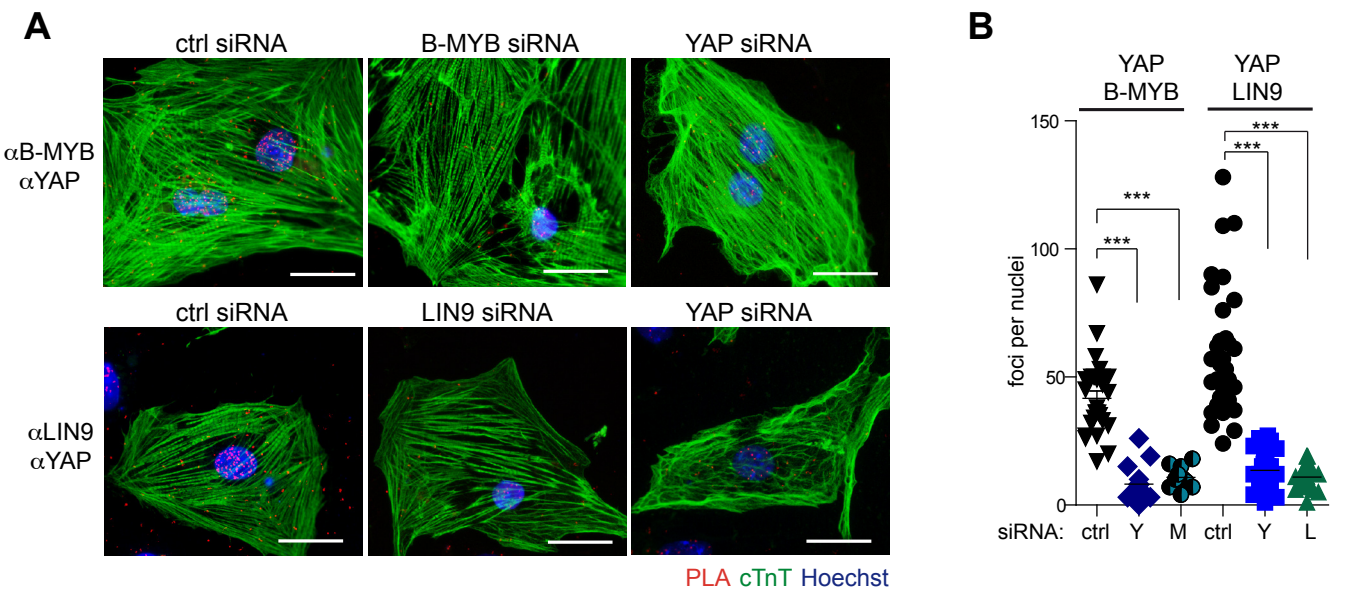

Figure 5

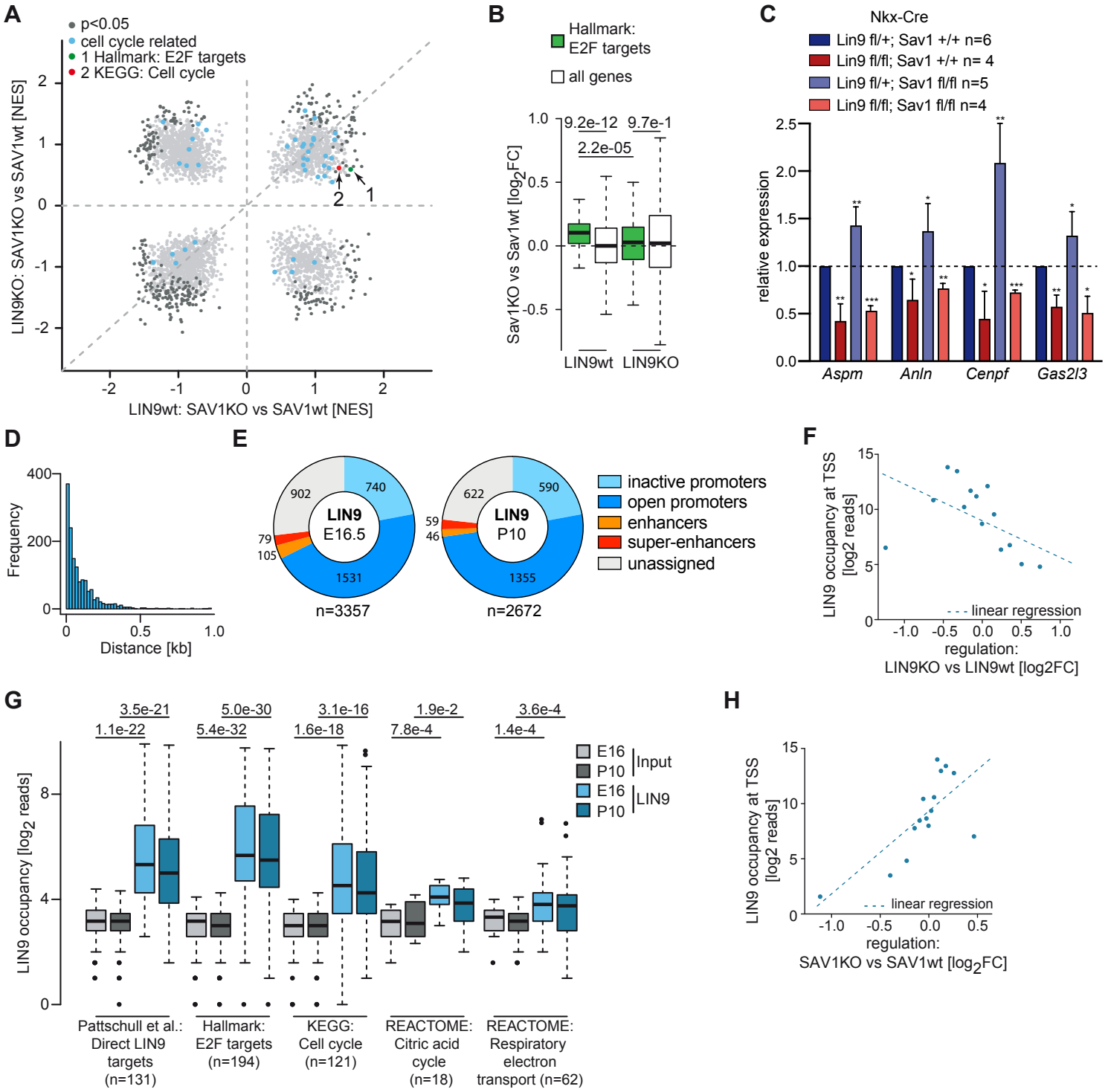

Figure 6

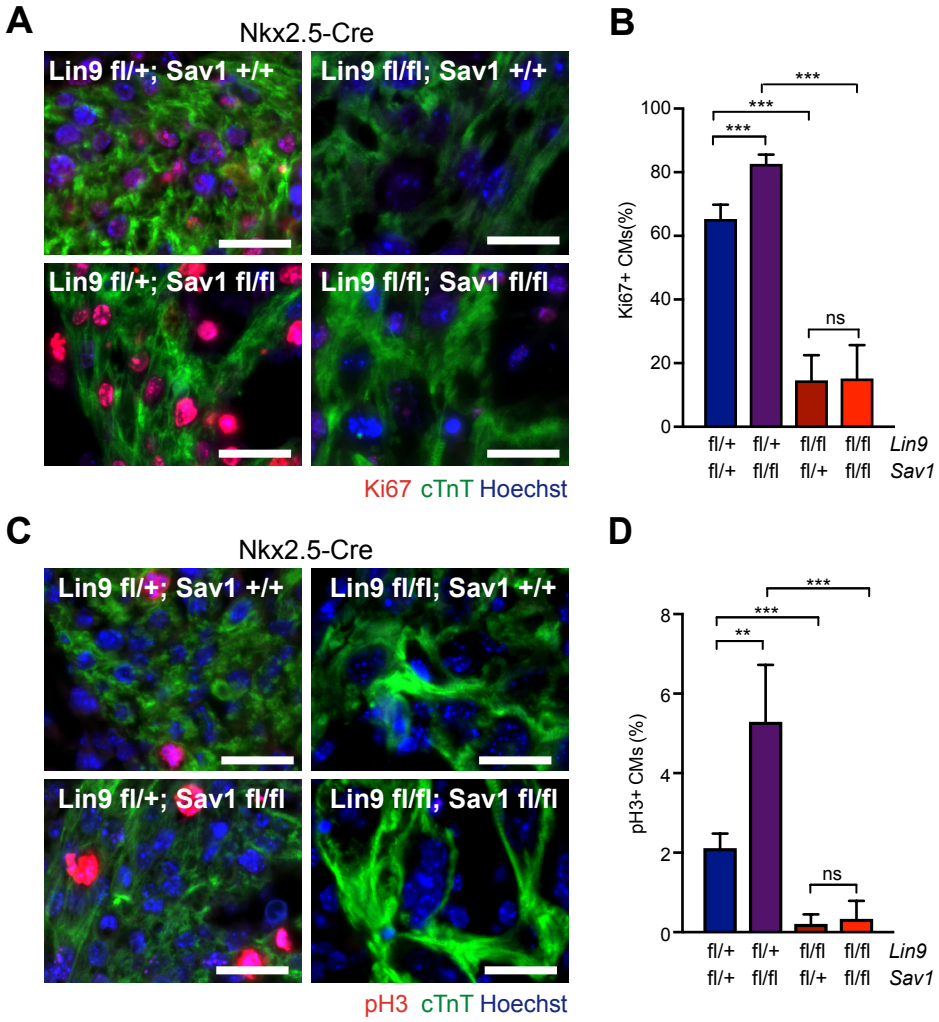

Figure 7

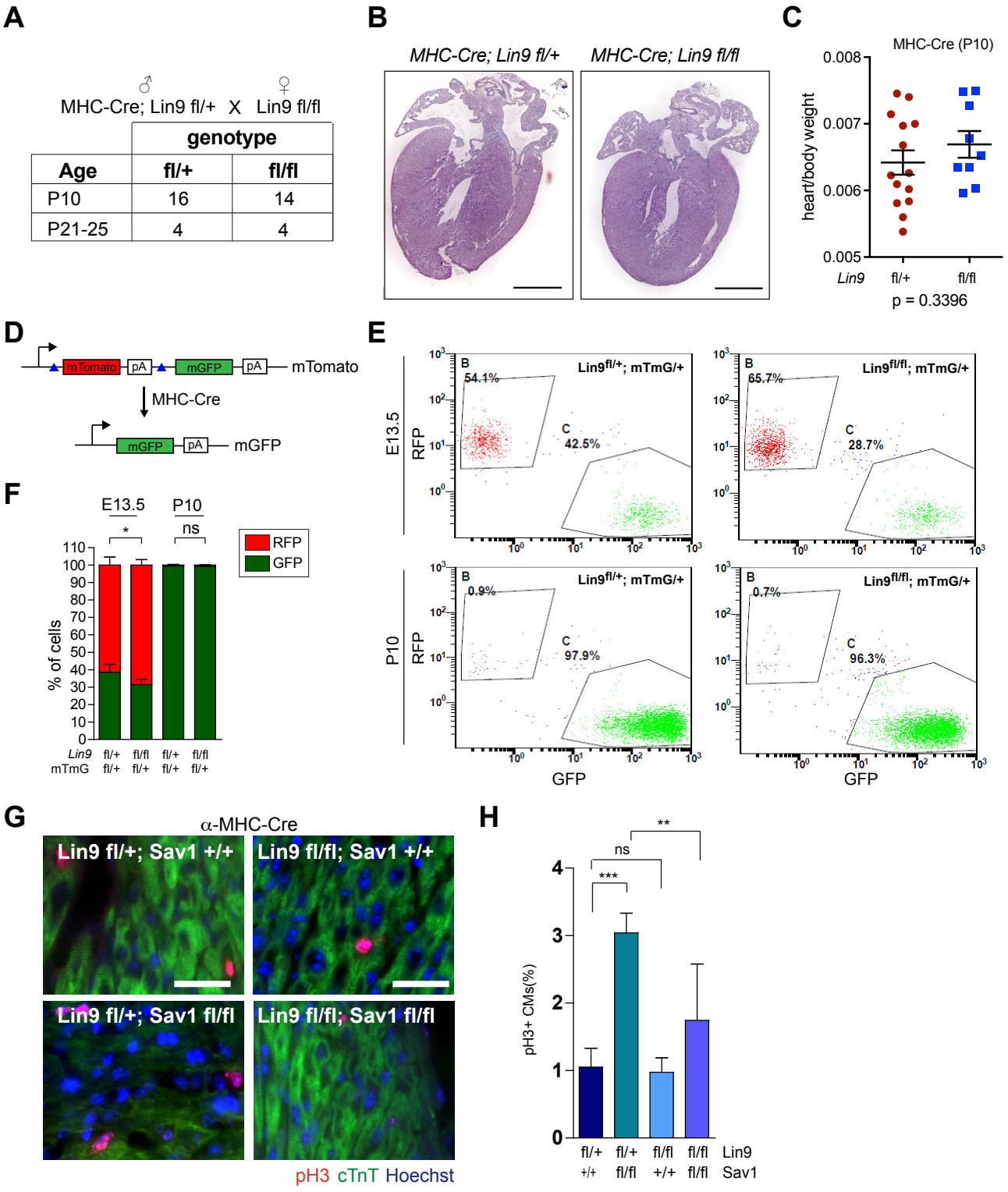

Figure 8